Mol Biol Rep (2012) 39:8793–8802
DOI 10.1007/s11033-012-1742-5

Biomimetic synthesis and characterization of cobalt nanoparticles using apoferritin, and investigation of direct electron transfer of Co(NPs)–ferritin at modified glassy carbon electrode to design a novel nanobiosensor

Soheila Kashanian · Fereshteh Abasi Tarighat · Ronak Rafipour · Maryam Abbasi-Tarighat

Received: 19 December 2011 / Accepted: 7 June 2012 / Published online: 1 July 2012

Abstract Oxyhydroxy cobalt CoO(OH) nanoparticles (Co-NPs) were prepared in horse spleen apoferritin (HsAFr) cavity. Transmission electron microscopy revealed the particle size was 5.5–6 nm. Mineralization effect on HsAFr was investigated by fluorescence and far-UV circular dichroism (far-UV CD) spectroscopies. The far-UV CD experiments indicated an increase in the α-helical content after mineralization. Intrinsic fluorescence data showed that mineralization acts as a quencher of HsAFr. For the first time, direct electron transfer between Co(NPs)–HsAFr and a glassy carbon electrode in the thin film of dihexadecylphosphate (DHP) was investigated by cyclic voltammetry (CV) to design a biosensor. The anionic surfactant DHP was used to achieve direct electron-transfer between Co(NPs)–HsAFr molecules and the GC electrode surface. CV result showed clearly a pair of well-defined and quasi-reversible redox peaks arise from Co(NPs)–HsAFr embedded in DHP film. This novel biosensor can be used in medical and industrial fields to detect different analytes.

S. Kashanian (✉)
Faculty of Chemistry, Sensor and Biosensor Research Center (SBRC) & Nanoscience and Nanotechnology Research Center (NNRC), Razi University, P.O. Box 67149 Kermanshah, Islamic Republic of Iran
e-mail: kashanian_s@yahoo.com

F. Abasi Tarighat
Department of Biology, Faculty of Science, Razi University, Kermanshah, Islamic Republic of Iran

R. Rafipour
Faculty of Chemistry, Razi University, Kermanshah, Islamic Republic of Iran

M. Abbasi-Tarighat
Department of Chemistry, Faculty of Sciences, Persian Gulf University, Bushehr, Islamic Republic of Iran

Keywords Nanoparticles · Biosensor · Direct electron transfer

Introduction

Nanomaterials are acquiring a big impact on development of electrochemical biosensors. Nanotechnology brings new possibilities for biosensors construction and for developing novel electrochemical bioassays. The electrochemical nanobiosensors were applied in areas of in clinical diagnosis, food technology, military, biomedical, industrial and environmental monitoring, and detection of infectious organisms [1–4].

Direct electrochemistry of redox proteins or enzymes has been the research focus for many years in views of the good model for mechanistic studies of their electron transfer activity in biological systems and serves as a foundation for fabricating electrochemical biosensors and bioreactors without using chemical mediators [5]. Unfortunately, it is difficult for the redox proteins to exchange electrons directly with electrode surface because of denaturation and loss of electrochemical activities occurred when the proteins adsorbed directly on the electrode surface. Therefore, finding new material with good biocompatibility for redox proteins immobilization on electrode surface is important to achieve their direct electrochemistry and keep their bioactivities [6]. Generally, modification of the electrodes surfaces by deposition of various films, including self-assembled monolayers (SAMs) [7], layer by layer assembly [8], electro-polymerization [9], covalent bonded immobilization [10] are effective methods to enhance the rate of electron transfer and obtain direct electrochemistry of redox enzymes or proteins. Successful examples have included cast films of proteins with insoluble surfactants [11], hydrogel polymers [12], biopolymers [13], clay [14], etc.

Some synthetic or natural surfactants can form ordered films featuring a stacked multibilayer structure on electrodes, which can incorporate redox proteins and facilitate reversible electron transportation. These surfactant films have the structure similar to that of biological membranes, and are viewed as biomembrane-like films [15]. Dihexadecyl phosphate (DHP) is a kind of anionic water insoluble surfactants with a negatively charged phosphatic head group and two long hydrocarbon chains [16]. Stable films can be made by casting DHP in chloroform onto electrodes [17]. Evaporation of the solvent leaves self-assembled multi-bilayer films, similar to stacks of biomembranes. Thus, DHP has been used to immobilize redox proteins onto the electrode surface to promote their electron transfer [17].

There is increasing interest in using biotemplates to develop the synthesis of nanoscale materials. Biomimetic synthetic routes offer the opportunity of controlling size, shape, crystal structure, orientation, and organization of nanoscale matter. Biotemplates such as oligonucleotides [18], peptides [19], and proteins [20, 21] offer rich structural and functional diversity to synthesize nanoparticles.

The horse spleen ferritin (HsAFr) is an iron storage protein consists of 24 subunits to form cage architecture of 12 nm diameter with an interior cavity of 8 nm diameter (Fig. 1) capable of accommodating up to 4,500 iron atoms [22]. Each subunit is an individual molecule that joins its neighboring subunits through noncovalent interactions; the subunits have a combined molecular weight of 474,000. The space group of apoferritin is F432 and it has six twofold symmetry axes, four three-fold symmetry axes and three fourfold symmetry axes. It is known that there are hydrophilic channels along the three-fold symmetry axes and hydrophobic channels along the fourfold symmetry axes [23]. Eight hydrophilic channels of about 4 Å are thought to facilitate the passage of metal ions and small molecules of appropriate size into the cavity of the protein

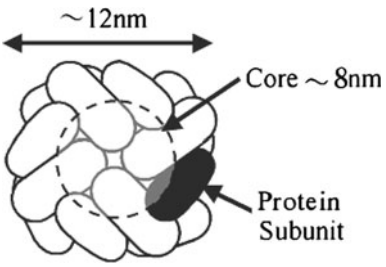

Fig. 1 Schematic drawing of ferritin molecule viewed down a fourfold axis. The spherical protein shell consists of 24 subunits. One subunit is colored *black* and the size of the core is shown as a *gray sphere*. The outer diameter of the shell is ~12 nm and the core size is 8 nm

or from the cavity to the external solution [24]. There are two types of subunits, the light-chain subunit (L subunit) and the heavy-chain subunit (H subunit), the relative ratio of which varies with the type of biological species and organ. The H subunit includes a catalytic ferroxidase site, which catalyzes the oxidation of Fe(II) to Fe(III), but this site is absent in the L chain subunit. In ferritin, oxidation of Fe(II) to Fe(III) leads to nucleation of iron oxide due to the insolubility of Fe(III) [25]. The assembled structure of ferritin is remarkably stable and robust, and able to withstand biologically extremes of high temperature (75–85 °C) and wide pH variations (2.0–12.0) for an appreciable period of time without significant disruption of their quaternary structure, which has allowed it to be used successfully as a template for constrained material synthesis [26].

Ferritin has a redox property, which is an unchangeable property when the electrochemical surrounding is fixed [27]. Since Ferritin has been extensively used as constrained reaction environments (nanoreactor) for synthesizing and encapsulation of various electroactive materials such as Ni, Co, Mn, Co:Pt, Pd, Pt, and CdS [25, 28–32], it can be used in biosensor and biofuel cell preparations, and biosensor development [7].

Protein electrochemistry has gained more interests in recent years for its potential applications in biosensors and bioreactors. The electron transfer reaction of ferritin has been studied using electrochemical and spectroscopic techniques. The electrochemical behavior of the physically adsorbed ferritin molecules on indium–tinoxide (ITO) glass was studied via cyclic voltammetry (CV) [33, 34]. The direct electron transfer of ferritin on a bare gold electrode was also evaluated [35]. Recently, electrochemical properties of SWNT/ferritin composite for bio-applications on the glassy carbon (GC) disk electrode was also studied [36]. Also electrochemical studies on ferritin immobilized onto a self-assembled monolayer-modified gold electrode have been already developed [27, 37–39]. The direct electron transfer of ferritin in DHP on an Au film electrode was also evaluated [40].

In this paper, we report successful synthesis of homogeneous oxyhydroxy cobalt CoO(OH) nanoparticles (Co-NPs) in the HsAFr cavity at buffering condition. The products of mineralization were characterized by spectroscopies and microscopy methods, and native polyacrylamide gel electrophoresis (PAGE). After synthesis, structural changes of HsAFr were studied using fluorescence and far-UV circular dichroism (far-UV CD) spectroscopies. Finally, for the first time, direct electron transfer between Co(NPs)–HsAFr and a GC electrode in thin film of DHP was investigated by CV to design of a new biosensor, which can be applied to detect biological and chemical analytes.

Materials and methods

Materials

Horse spleen apoferritin (HsAFr) was purchased from Callbiochem. All chemical were purchased from Sigma-Aldrich and used as received with no further purification.

Synthesis and characterization of cobalt core in the HsAFr cavity

Synthesis

The HsAFr solution (1 mg/mL) was prepared, and then dialyzed against 100 mM HEPES (2-[4-(2-hydroxyethyl)piperazin-1-yl]ethanesulfonic acid) buffer containing 60 mM of NaCl (pH 8.5–8.7). At room temperature solutions of $Co(OAc)_2{\cdot}4H_2O$ (25 mM, 675 μL) and H_2O_2 (3 %, 18 μL) were added over a 2 h period with 15 min intervals, while adjusting the pH with 0.01 M of NaOH during synthesis. Theoretical loading of 1,500 Co per HsAFr molecule was achieved by 15 addition cycles. After each cycle, UV–Vis spectrum of sample was measured on an Agilent 8453 spectrophotometer. The solution after Co(NPs) synthesis was centrifuged at a speed of 3,000 rpm for 20 min. The supernatant was further centrifuged at a speed of 6,000 rpm for 60–80 min such that an unnecessary bulk material was precipitated and removed. At this time, Co(NPs)–HsAFr were dispersed in the supernatant. Proteins in the supernatants were quantified by Bradford-assay to estimate the loss of proteins and the protein ratio, [protein in the supernatant]/[initial apoferritin], was calculated as yield of protein ratio (YPR) [41].

Characterization of Co(NPs)

The morphology and particle size distributions of the iron oxide cores of Co-NPs were determined by transmission electron microscopy (TEM) (OBURI, model LEO 906). Several microliters of the supernatant were put on the carbon film coated cupper for TEM, and excessive solution was removed. The samples were negatively stained by 3 % aurothioglucose. Aurothioglucose did not stain the cavity because steric hindrance prevented it from going through the channels [25]. Thus, we could distinguish apoferritin and ferritin by aurothioglucose negative staining. Furthermore, Co(NPs)–HsAFr in the supernatants were observed by TEM to measure core formation ratio (CFR), which is represented as:

$$\mathrm{CFR}\ (\%) = [\mathrm{Co(NPs)} - \mathrm{HsAFr}]/[\mathrm{HsAFr}]_{\mathrm{total}}, \quad (1)$$

where [Co(NPs)–HsAFr] is the number of Co(NPs)-incorporated HsAFr and $[\mathrm{HsAFr}]_{\mathrm{total}}$ is the total number of [HsAFr] and Co(NPs)-incorporated HsAFrs. The efficiency of core formation (ECF) was calculated by multiplying YPR and YCF [41].

An electrophoresis experiment was run for both the HsAFr and preparations of Co(NPs)–HsAFr protein cages using 6 % polyacrylamide gels under native (non-denaturing) conditions. Gels were stained for protein using Coomassie blue and stained for Co using 1-nitroso-2-naphthol-3,6-disulfonic acid (50 mM in 1:1 H_2O: MeOH) [42].

Infra-red (IR) spectra (KBr) of the samples were collected using an ABB Bomem Mb103 spectrometer.

Study of structural changes of Co(NPs)–HsAFr

Spectrofluorimeter studies

Fluorescence emission measurements were carried out with a JASCO spectrofluorimeter (FP 6200) using a 1 cm pathlength quartz cuvette at 25 °C. HsAFr and Co(NPs)–HsAFr solution were prepared by diluting stock solutions to 1.5 μM. Intrinsic fluorescence emission spectra were recorded at 300 ± 400 nm with the excitation wavelength set at 295 nm. Experiments for extrinsic fluorescence emission spectra, using anilinonaphthalene-8-sulfonic acid (ANS) were performed by incubating the proteins and ANS (0.03 mM) for 30 min prior to the measurements. Blanks, without protein samples, were subtracted from the spectra.

Circular dichroism studies

Circular dichroism (CD) spectra were collected on a Jasco J-810 spectropolarimeter. The instrument was periodically calibrated with (+) 10-camphorsulphonic acid. Quartz cells having path lengths of 0.1 cm were used, and the scanning speed was set at 100 nm/min. The far-UV CD spectra were measured protein concentration of 0.5 mg/1 mL for both HsAFr and Co(NPs)–HsAFr at room temperature over a wavelength range of 250 to 190 nm. Appropriate buffer solutions running under the same conditions were taken as blanks, and their contributions were subtracted from the experimental spectra.

Design a new biosensor based direct electron transfer between Co(NPs)–HsAFr in thin film of DHP

Preparation of (Co(NPs)–HsAFr)–DHP film

The GC, 2 mm in diameter, electrode was polished carefully with 1.0, 0.3 and 0.05 mm alumina slurry and sonicated in water and absolute ethanol, respectively. Finally, the GC electrode was thoroughly rinsed with water and dried in air.

DHP films were made by casting 8 μL of 0.05 M DHP in chloroform onto GC electrode. Chloroform was evaporated in air. DHP-coated GC electrode was then placed into 1.6 mg mL^{-1} Co(NPs)–HsAFr solution, over-night or longer for incorporation of Co(NPs)–HsAFr. The (Co(NPs)–HsAFr)–DHP film was then dried in air overnight.

Cyclic voltammetry

CV measurements were performed with a computer controlled autolab (SAMA), in a conventional three-electrode electrochemical cell with the modified GC electrode as the working electrode, a large platinum wire as the auxiliary electrode, and Ag/AgCI (saturated KCI) electrode as the reference electrode. The CV measurements were performed at 20 °C.

Topography analysis of (Co(NPs)–HsAFr)–DHP film using atomic force microscopy (AFM)

Immobilization of Co(NPs)–HsAFr in DHP film on GC electrode surface was examined by AFM. Images were obtained with the explorer atomic force microscope, which was in non contact mode, using high resonance frequency (S0 = 170 kHz) pyramidal with silicon probes having dynamic force.

Results and discussion

Cobalt core formation Studies

The formation of Co-NPs with theoretical loading of 1,500 Co per HsAFr molecule was conducted in HEPES buffers at pH 8.5–8.7 using H_2O_2 as the oxidant. Douglas et al., reported Co(O)OH core formation in the HsAFr by oxidizing Co(II) with H_2O_2 while the reaction solution was run unbuffered at pH 8.5, and the proton generated during hydrolysis was titrated dynamically with 10 mM NaOH [43]. Allen et al. [42] also made Co_3O_4 and Co(O)OH cores in the protein cage from *Listeria innocua* by dynamic titration with 50 mM NaOH. However, Tsukamoto et al. showed the pH control using a buffer agent is much simpler and more suitable for mass-production [28]. They made Co_3O_4 cores in the HsAFr and recombinant apoferritin composed of L-subunits using buffered reaction solutions. Some buffer reagents strongly react with the cobalt ions and hinder the biomineralization. Therefore, they surveyed different buffer agents (Tris, TES, Bis–Tris, Phosphate, CHES, MOPS and HEPES). In this study as mentioned above HEPES was used as buffer agent.

In the presence of the HSAFr cages, reactions proceeded to form homogeneous olive green solutions. In contrast, reactions in the absence of the HsAFr cages resulted in the bulk precipitation of olive green solids. The lack of precipitate in the reactions containing the HsAFr cages, and the strong color present in these solutions, suggested that the oxidative hydrolysis of Co(II) occurred in a spatially selective manner within the confines of the protein cage [42]. The reactions could be followed by monitoring the change in the UV–Vis absorbance at each step (Fig. 2). The UV–Vis spectra exhibited well-defined peaks at 350 nm corresponding with cobalt oxides, most likely cobalt oxyhydroxide CoO(OH) [43, 44] (Fig. 2a). As the number of Co in HsAFr was increased the absorption bond at 350 nm was shifted to higher wavelengths (Fig. 2b).

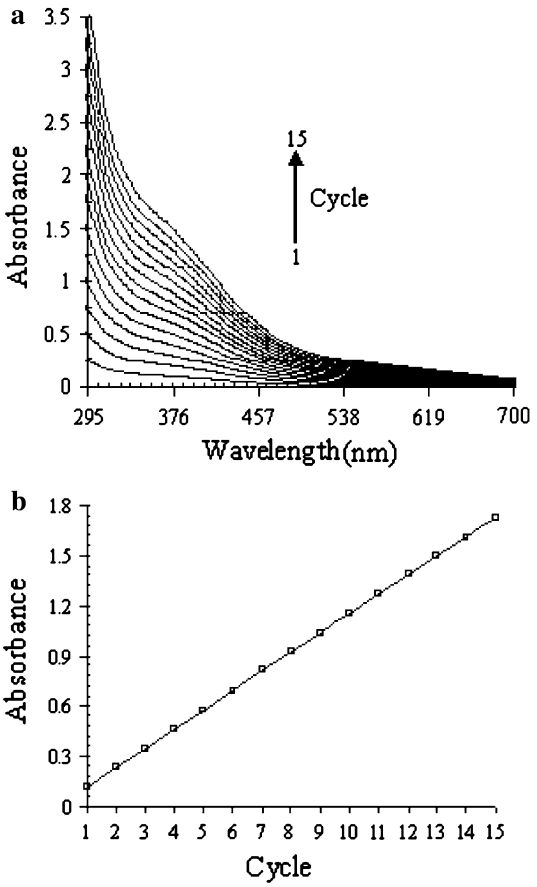

Fig. 2 **a** Time course for the synthesis of Co(NPs)–HsAFr (15 min reagent addition), monitored by UV–Vis spectroscopy by 15 addition cycles. **b** Absorbance changes at 350 nm on each step

HsAFr and Co(NPs)–HsAFr were electrophoretically analyzed on the polyacrylamide gel (PAGE), under native (non-denaturing) conditions (Fig. 3). The co-migration of the samples both HsAFr and Co(NPs)–HsAFr indicates that the overall charge on the exterior of the HsAFr and the Co(NPs)–HsAFr has not been measurably altered during the synthesis, that the Co(III) atoms are indeed to the protein shell.

IR spectra (KBr pellet) of precipitate showed strong band at 587 cm^{-1} characteristic of Co(O)OH, which was indicative to Co–O stretching frequency [43].

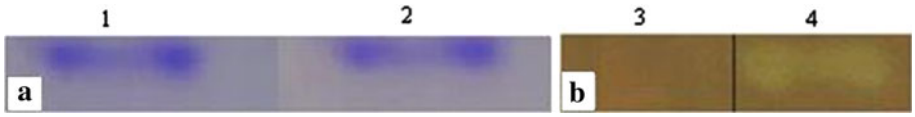

Fig. 3 Native polyacrylamide gel electrophoresis stained; **a** for protein using Coomassie Blue, and **b** for cobalt using 1-nitroso-2-naphthol. *Lane 1* HsAFr, *lane 2* Co(NPs)–HsAFr, *lane 3* HsAFr, *lane 4* is Co(NPs)–HsAFr

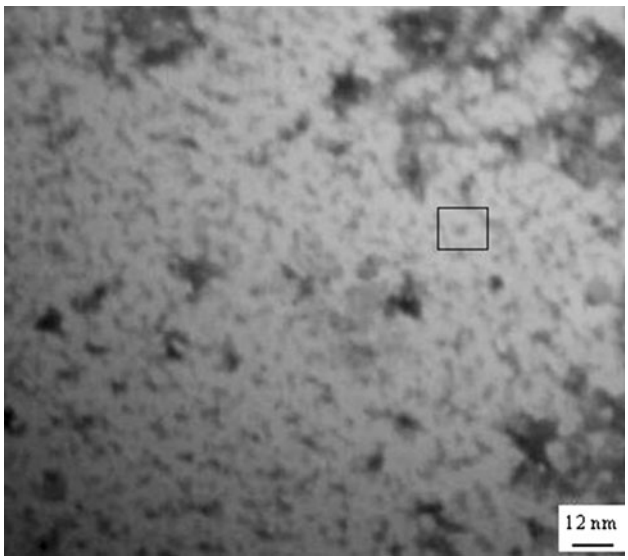

Fig. 4 A representative TEM image of Co(NPs)–HsAFr negatively unstained with uranyl acetate. The presence of cobalt nanoparticles has been indicated in *black squares*. The *scale-bar* is 12 nm

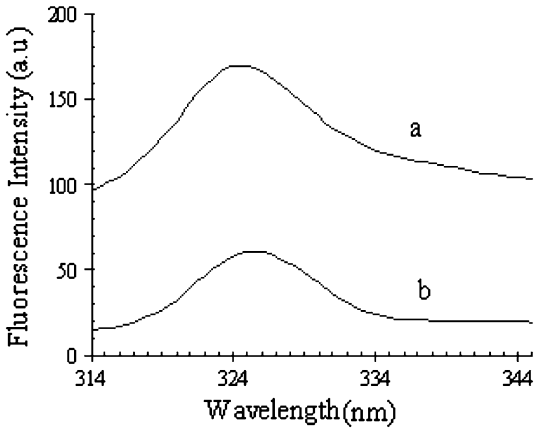

Fig. 5 Intrinsic fluorescence spectra of HsAFr (1.5 μM) (*a*), and Co(NPs)–HsAFr (1.5 μM) (*b*). The excitation wavelength was set at 295 nm

TEM images of samples negatively stained with uranyl acetate confirmed that the particles were actually produced within the HsAFr cavity (Fig. 4). Uranyl acetate penetrated the ion-channel of aoferritin and stained the inner cavity [25], therefore when samples were negatively stained with uranyl acetate, the intact protein cage was clearly visible as white 'halo' surrounding the Co oxides cores on the interior surface. The presence of the apoferritin coat prevents irreversible aggregation of the particles and their precipitation. Negatively stain of the materials indicated, as expected, an intact protein shell surrounding the mineral core. The particle size was measured and found to be monodisperse with an average diameter of 5.5–6 nm and generally spherical in shape. YPR (%) and CFR (%) were calculated to be 95 and 99 %, respectively. ECF (Multiplying YPR and CFR) was calculated to be 94 %. These data strongly suggest that the Co(NPs)–HsAFr is structurally intact and also no degradation occurs during chemical functionalization of the protein shell.

Spectroscopic studies

Intrinsic fluorescence studies

Intrinsic fluorescence spectra of HsAFr and Co(NPs)–HsAFr (Fig. 5) exhibited an emission maximum at approximately the same wavelength (326 nm) of both HsAFr and Co(NPs)–HsAFr when both proteins were excited at 295 nm without any shifts in the wavelength. The fluorescence emission in HsAFr was higher than that of Co(NPs)–HsAFs. Therefore, tryptophan fluorescence can be quenched by apoferritin mineralization.

Extrinsic fluorescence studies

The aromatic chromophore ANS is feebly fluorescent in water, but its spectrum is blue shifted and its intensity is dramatically increased in nonpolar solvents or when it binds to nonpolar sites of proteins [45–47]. ANS binding assays were performed to study the occurrence of exposed hydrophobic surfaces in HsAFr and Co (NPs)–HsAFr. The extrinsic fluorescence spectra of ANS, HsAFr and Co(NPs)–HsAFr (Fig. 6) exhibited an emission maximum at approximately the same wavelength (523 nm) for both HsAFr and Co(NPs)–HsAFr when both proteins were excited at 360 nm without any shifts in wavelength. This result is indicative of no detectable changes in apoferritin after mineralization.

Far-UV circular dichroism studies

Proteins exhibit characteristic CD spectra in the Far-UV region and the appearance of these spectra are related to the presence of secondary structure. Accordingly, CD is frequently used to

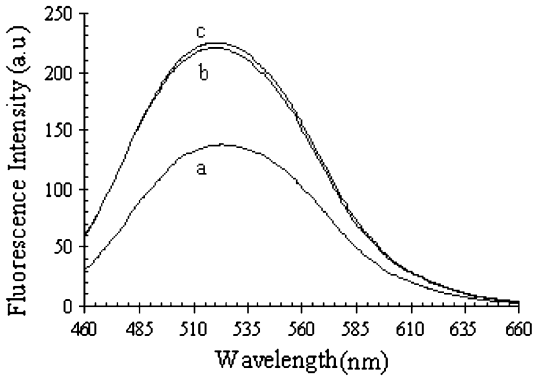

Fig. 6 The extrinsic fluorescence spectra of ANS (0.3 mM) (*a*), HsAFr (1.5 μM) (*b*), and Co(NPs)–HsAFr (1.5 μM) (*c*). The excitation wavelength was set at 360 nm

Table 1 The secondary structure of HsAFr and Co(NPs)–HsAFr

	α-helix (%)	β-sheet (%)	Turn (%)	Random (%)
HsAFr	75	2.5	18	4.5
Co(NPs)–HsAFr	84	0	11.5	4.5

estimate the fractions of various types of secondary structure in proteins [48]. Far-UV CD was used in the analysis of Co-NPs as a spectroscopic probe which is sensitive to protein secondary structure. The result showed that the secondary structure of Co(NPs)–HsAFr, with an increase of 9 % in the α-helical content and a decrease in β-sheet and turns structures (Table 1). The Far-UV experiments indicated that mineralization of HsAFr causes more stability of the protein structure with an increment in the α-helical content.

Designing of a new biosensor based Co(NPs)–HsAFr in thin film of DHP

Direct electrochemistry of Co(NPs)–HsAFr in DHP film

Horse spleen ferritin is negatively charged at pH 7.0, since its isoelectic point (PI) is 4.5. It was found that cationic surfactant, such as DSAB, caused ferritin to be precipitated when it was mixed with ferritin. Thus, ferritin can only be mixed with neutral and anionic surfactants [40], Wu and his co-workers showed that ferritin in dihexadecylphosphate (DHP) (an anionic surfactant) film gave a well-defined pair of redox peaks in the buffer without ferritin. They suggested, it might contribute to two hydrophobic tails of DHP. They showed, when an Au film electrode coated with DHP film was placed in ferritin solution, CV scanning for several hours gave only relatively small redox peaks. They suggested, the charges of DHP can block ferritin penetration through the film [40]. Thus we chose DHP in our experiments

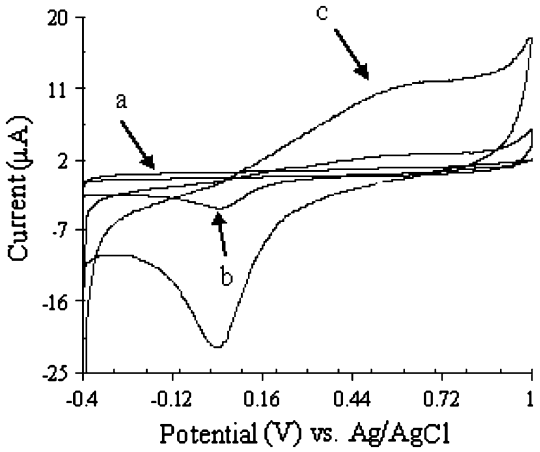

Fig. 7 Cyclic voltammograms: (*a*) bare GC electrode in pH 8.0 buffer containing 1.6 mg mL^{-1} Co(NPs)–HsAFr, (*b*) DHP film on GC electrode in 1.6 mg mL^{-1} Co(NPs)–HsAFr in pH 8.0 buffer; (*c*) Co(NPs)–HsAFr–DHP cast onto GC electrode in pH 8.0 buffer containing no Co(NPs)–HsAFr, scan rate: 100 mV s^{-1}

CV was used to investigate the direct electron transfer between Co(NPs)–HsAFr and a GC electrode in thin film of DHP (Fig. 7). No CV peaks are observed on a bare GC electrode in a 1.6 mg mL^{-1} of Co(NPs)–HsAFr solution in pH 8.0 buffer solution at potential range of −0.4 to 1 V (Fig. 7a). This shows that electron transfer between the electrode and Co(NPs)–HsAFr in this solution occurs very slowly or not at all.

When a GC electrode coated with DHP film was placed in 1.6 mg mL^{-1} of Co(NPs)–HsAFr, repetitive CV scanning for several hours gave small redox peaks (Fig. 7b). This suggests that only a small amount of Co(NPs)–HsAFr diffuses into the DHP film. The negative charges of DHP can block the entering of Co(NPs)–HsAFr into the film [40].

However, (Co(NPs)–HsAFr)–DHP films, gave a well-defined pair of redox peaks (Fig. 7c) in the buffer solution without Co(NPs)–HsAFr. It is no doubt that the peaks arise from the embedded Co(NPs)–HsAFr in the film. From the CV results the anodic (Epa) and cathodic (Epc) peak potentials were obtained as 0.002 V and 0.540 V (vs. AG/AgCl), respectively. The apparent formal potential ($E^{0\prime}$), which was calculated from the equation as $E^{0\prime} = (Epa + Epc)/2$, was got as 0.280 V (vs. Ag/AgCl), and ratio of anodic to cathodic peak currents is about one. The peak-to-peak potential separation (ΔEp) at 100 mV/s was 0.538 V, in contrast to the much larger peak potential difference reported for Ferritin in DHP on an Au film electrode. The large peak may be ascribed to the immobilization of protein molecules in an abnormal orientation [49]. These data support one point that the direct electrochemistry of Co(NPs)–HsAFr–DPH film considered to proceed by a quasi-reversible redox reaction. This anionic surfactant DHP has good biocompatibility and could provide

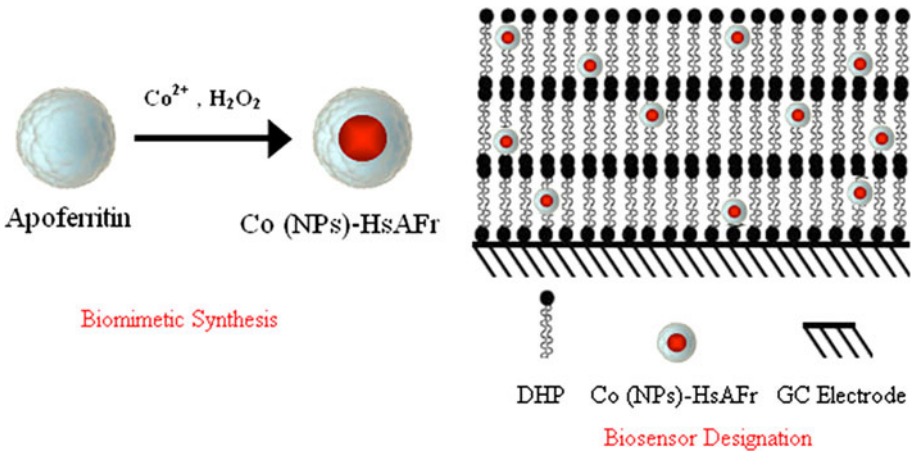

Fig. 8 Scheme representation of the process of Co(NPs)–HsAFr immobilization in DHP film on GC electrode surface

appropriate microenvironment for Co(NPs)–HsAFr to perform direct electrode-transfer with the electrode surface, and then could facilitate the electron transfer process between redox group of Co(NPs)–HsAFr and GC electrode surface.

DHP, a surfactant with a negative charged headgroup and two nonpolar tails, is insoluble in water and does not form micelles. Stable films can be made by casting DHP in chloroform onto electrodes (Fig. 8) [17]. Evaporation of the solvent leaves self-assembled multi-bilayer films, similar to stacks of biomembranes. This unique structure is very similar to the structure of biological membranes, in which the constituent lipids are arranged in the tail-to-tail configuration with the hydrophilic head groups toward outside and proteins are adsorbed onto the surface of or imbedded into the layers [16]. These ordered multi-bilayer films were presumably stabilized mainly by hydrophobic interactions between the protein and film components. The immobilization of Co(NPs)–HsAFr onto GC surface can help the protein to keep a favored orientation or to make possible conducting channels between the prosthetic groups and the electrode surface, and they will both reduce the effective electron transfer distance, thereby facilitating electron transfer between electrode and protein.

These results suggest that the electroactive HsAFr–Co(II) within the DHP film is converted to HsAFr–Co(III) on the forward scan to positive potential and vice versa.

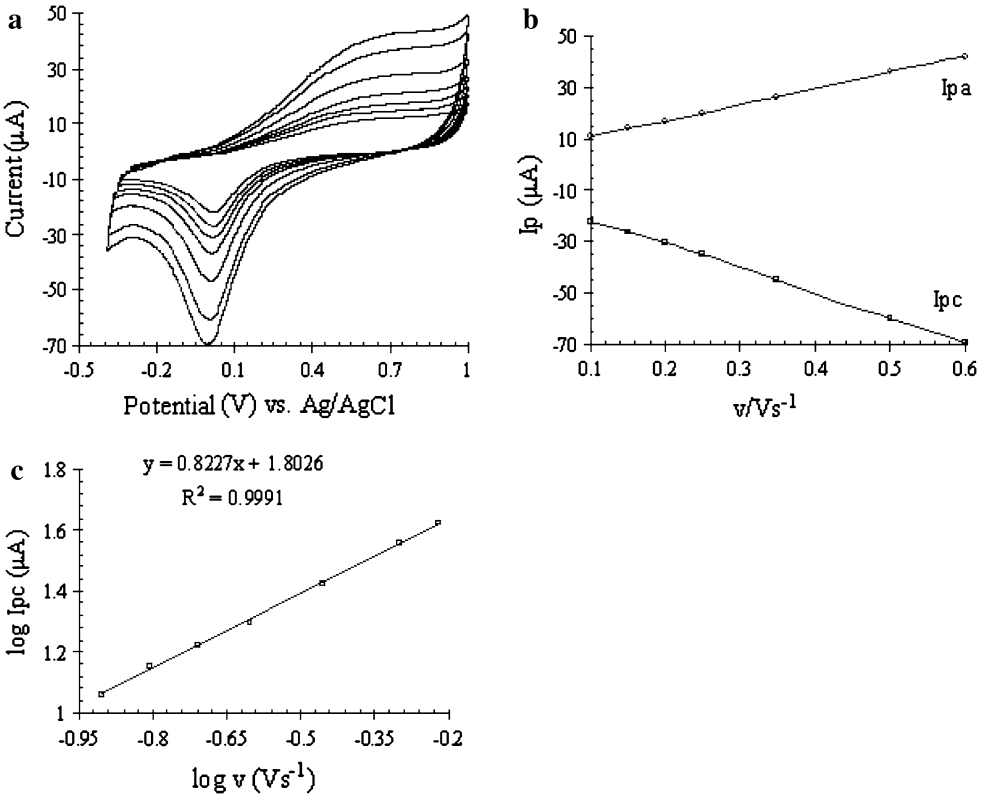

Fig. 9 **a** Cyclic voltammograms of Co(NPs)–HsAFr in the DHP film in pH 8.0 buffer solution with different scan rates: 100, 150, 200, 250, 350, 500, 600 mV s^{-1}, **b** calibration plot of cathodic and anodic peak currents versus scan rates, and **c** The logarithmic relation of cathodic peak currents vs. scan rate for Co(NPs)–HsAFr in DHP film in pH 8.0 buffer solution

The influence of scan rate on the cyclic voltammetric response of (Co(NPs)–HsAFr)–DHP film was further recorded with the results shown in Fig. 9. Figure 9a demonstrates typical cyclic voltammograms of (Co(NPs)–HsAFr)–DHP film with scan rates from 0.1 to 0.6 Vs^{-1} (vs. Ag/AgCl). With the increase of the scan rates, the cathodic and anodic peak currents of (Co(NPs)–HsAFr)–DHP increased simultaneously, meanwhile the cathodic and anodic peak potentials showed a small shift and the peak to peak separation also increased. As shown in Fig. 9b, the cathodic and anodic peak currents increased linearly with the scan rates from 0.1 to 0.6 V s^{-1}. This revealed that the electron transfer between Co(NPs)–HsAFr and the GC electrode could be easily performed in DHP film. Figure 9c showed the linear relation between log (Ipc) and log υ, its slop is 0.8227. As it is known, for ideal diffusion-controlled reaction, the slop is 0.5; for ideal thin layer electrochemistry, the slope is 1 [50]. In this study, the slop is 0.8227, which indicates that both diffusion control and surface control exist in the reaction course. When the Co(NPs)–HsAFr–DHP film was stored in air at room temperature, the peak currents only decreased about 10 % after 30-day period. The good long-term life may be attributed to the strengthened biocompability and stability of the Co(NPs)–HsAFr–DHP film.

Study on the release and uptake of iron in the core of Co(NPs)–HsAFr

EDTA is a powerful complexing agent of Co(II). Therefore, it can be used to investigate the exit and entry of Co(II) in the HsAFr by CV. Figure 10 shows the cyclic voltammogram of Co(NPs)–HsAFr–DHP film when the electrode immersed in pH 8.0 phosphate buffer containing 10 mM of EDTA. In the first scan, the cathodic peak

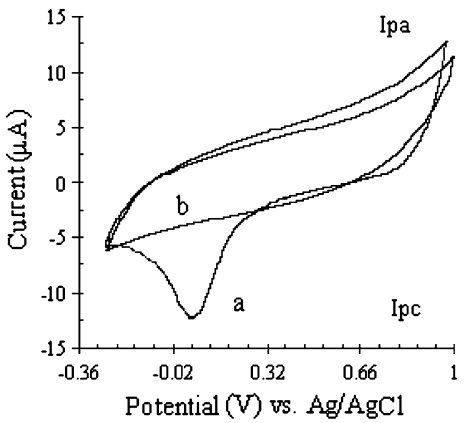

Fig. 10 Cyclicvoltammograms of (Co(NPs)–HsAFr)–DHP film on glassy carbon electrode in pH 8.0 buffer in the presence of 10 mM EDTA. The first scan (**a**), the second scan (**b**), scan rate: 100 mV s^{-1}

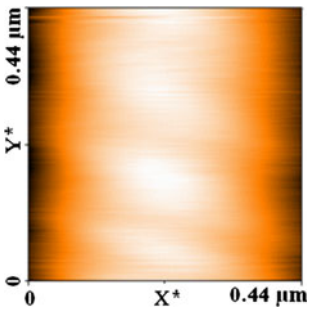

Fig. 11 AFM (non-contact mode) image of the bare glassy carbon electrode

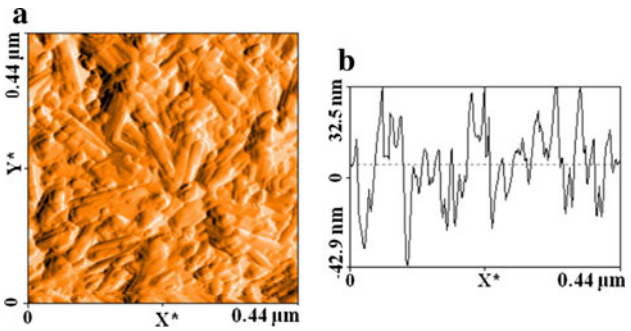

Fig. 12 AFM (non-contact mode) image of the (Co(NPs)–HsAFr)–DHP film on glassy carbon electrode (**a**). The cross section view to the *line* drawn (**b**)

remains at 0.05 V, but the anodic peak disappears (Fig. 10a). In the second scan, both the cathodic and anodic peaks are missing (Fig. 10b) and this phenomenon keeps the same in the following scans. It indicated that in the first scan the reduced cobalt exited from the core and chelated by EDTA. The cobalt did not enter the core of the HsAFr and caused the absence of the cathodic and anodic peaks in the following scans.

Topograghy analysis of Co(NPs)–HsAFr–DHP film using atomic force microscopy

Figure 11 shows non-contact AFM images of a bare GC electrode surface. The bare GC electrode had no impurity on its surface, as shown in Fig. 11. Figure 12a shows the AFM image of Co(NPs)–HsAFr–DHP film on GC electrode. The roughness of the surface increased significantly as compared to that of the bare GC electrode, indicating successful formation of biomembrane like lipid (DHP) on the GC electrode surface. The cross section view (Fig. 12b) showed that the dimension of (Co(NPs)–HsAFr)–DHP film on GC electrode is approximately 40 nm. Also, result from CV experimental clearly showed that a well-defined pair of redox peaks arises from embedded Co(NPs)–HsAFr in DHP film.

Conclusion

Co nanoparticles were successfully synthesized in the HsAFr cavity using HEPES as a buffer agent with theoretical loading of 1,500 Co per HsAFr molecule.

TEM analysis confirmed that the minerals were encapsulated inside the protein. Under the range of synthesis conditions the protein cage remains unaltered.

Taking all of the information obtained into consideration, the Co(NPs) formation has occurred by this process: Co (II) ions are attracted by the negatively charged threefold channel and go through the threefold channels into the apoferritin cavity and formed chemical bonds with the functional groups in the interior wall of the ferritin during the oxidation process of the metal ions [51].

The effect of mineralization on the structure of HsAFr was investigated by spectroscopic techniques including fluorescence and CD spectroscopies. Intrinsic fluorescence data showed that the mineralization acts as a quencher of the HsAFr, and extrinsic fluorescence data revealed the hydrophobic binding site at the surface of HsAFr was not changed. The Far-UV CD experiments indicated that mineralization causes an increase in the α-helical content, which makes the protein more stable.

In this paper, we report for the first time, quasi and direct electron transfer between Co(NPs)–HsAFr molecules and GC electrode surface without the aid of any electron mediator by immobilizing an anionic surfactant DHP cast on GC electrode surface. These ordered biomembrane like lipid films are presumably stabilized mainly by hydrophobic interactions between Co(NPs)–HsAFr and DHP film. The reason for facilitating the direct electron transfer between Co(NPs)–HsAFr and GC electrode surface is due to DHP inhibition of Co(NPs)–HsAFr adsorption onto bare electrode. The adsorption often results in the proteins and other macromolecules denaturation, and can create an insulating layer which inhibits passage of electrons [50].

With the aid of cobalt chelator, EDTA, the exit and entry of cobalt in HsAFr core was studied by CV. It was found that reduced cobalt could exit HsAFr core and was chelated by EDTA. AFM image of Co(NPs)–HsAFr–DHP film on GC electrode showed successful formation of biomembrane like lipid (DHP) on the GC electrode surface.

Therefore, we could design a new biosensing devise based direct electron transfer between Co(NPs)–HsAFr and GC electrode in thin film of DHP, which can be used to detect and determine chemical and biological analytes in different areas such as healthcare, industry, agri-food, environment, etc.

References

1. Pumera M, Sánchez S, Ichinose I, Tang J (2007) Electrochemical nanobiosensors. Sens Acuators B 123:1195–1205
2. Omidfar K, Kia S, Kashania S, Paknejad M, Besharatie A, Kashanian S, Larijani B (2010) Colloidal nanogold-based immunochromatographic strip test for the detection of digoxin toxicity. Appl Biochem Biotechnol 160:843–855
3. Omidfar K, Dehdast A, Zarei H, Khorsand Sourkohi B, Larijani B (2011) Development of urinary albumin immunosensor based on colloidal AuNP and PVA. Biosens Bioelectron 26:4177–4183
4. Omidfar k, Rasaee MJ, Zaraee AB, Amir MP, Rahbarizadeh F (2002) Stabilization of penicillinase–hapten conjugate for enzyme immunoassay. J Immunoassay Immunochem 23(2002): 385–398
5. Zheng N, Zhou X, Yang W, Li X, Yuan Z (2009) Direct electrochemistry and electrocatalysis of hemoglobin immobilized in a magnetic nanoparticles-chitosan film. Talanta 79:780–786
6. Zhang Y, Zheng J (2008) Direct electrochemistry and electrocatalysis of myoglobin immobilized in hyaluronic acid and room temperature ionic liquids composite film. Electrochem Commun 10:1400–1403
7. Park CW, Park HJ, Kim JH, Won K, Yoon HH (2009) Immobilization and characterization of ferritin on gold electrode. Ultramicroscopy 109:1001–1005
8. Wang G, Liu Y, Hu N (2007) Comparative electrochemical study of myoglobin loaded in different types of layer-by-layer assembly films. Electrochim Acta 53:2071–2079
9. Li C (2006) Voltammetric determination of tyrosine based on an L-serine polymer film electrode. Colloid Surf B 50:147–151
10. Patolsky F, Weizmann Y, Willner I (2004) Long-range electrical contacting of redox enzymes by SWCNT connectors. Angew Chem Int Ed 43:2113–2117
11. Liu X, Zhang W, Huang Y, Li G (2004) Enhanced electron-transfer reactivity of horseradish peroxidase in phosphatidylcholine films and its catalysis to nitric oxide. J Biotechnol 108:145–152
12. Shen L, Huang R, Hu N (2002) Myoglobin in polyacrylamide hydrogel films: direct electrochemistry and electrochemical catalysis. Talanta 56:1131–1139
13. Zhang Y, Zheng J (2008) Direct electrochemistry and electrocatalysis of cytochrome c based on chitosan-room temperature ionic liquid-carbon nanotubes composite. Electrochim Acta 54:749–754
14. Liu Y, Liu H, Hu N (2005) Core-shell nanocluster films of hemoglobin and clay nanoparticle: direct electrochemistry and electrocatalysis. Biophys Chem 117:27–37
15. Liu H, Wang L, Hu N (2002) Direct electrochemistry of hemoglobin in biomembrane-like DHP–PDDA polyion–surfactant composite films. Electrochim Acta 47:2515–2523
16. Shan W, Liu H, Shi J, Yang L, Hu N (2008) Self-assembly of electroactive layer-by-layer films of heme proteins with anionic surfactant dihexadecyl phosphate. Biophys Chem 134: 101–109
17. Zhang Z, Rusling JF (1997) Electron transfer between myoglobin and electrodes in thin films of phosphatidylcholines and dihexadecylphosphate. Biophys Chem 63:133–146
18. Liu DG, Gugliotti LA, Wu T, Dolska M, Tkachenko AG, Shipton MK, Eaton BE, Feldheim DL (2006) RNA-mediated synthesis of palladium nanoparticles on Au surfaces. Langmuir 22(5862): 5866
19. Sewell SL, Wright DW (2006) Biomimetic synthesis of titanium dioxide utilizing the R5 peptide derived from *Cylindrotheca fusiformis*. Chem Mater 18:3108–3113

20. Liu G, Wu H, Dohnalkova A, Lin Y (2007) Apoferritin-templated synthesis of encoded metallic phosphate nanoparticle tags. Anal Chem 79:5614–5619
21. Iwahori K, Enomoto T, Furusho H, Miura A, Nishio K, Mishima Y, Yamashita I (2007) Cadmium sulfide nanoparticle synthesis in Dps protein from *Listeria innocua*. Chem Mater 19:3105–3111
22. Uchida M, Flenniken ML, Allen M, Willits DA, Crowley BE, Brumfield S, Willis AF, Jackiw L, Jutila M, Young MJ, Douglas T (2006) Targeting of cancer cells with ferrimagnetic ferritin cage nanoparticles. J Am Chem Soc 128:16626–16633
23. Iwahori K, Yoshizawa K, Muraoka M, Yamashita I (2005) Fabrication of ZnSe nanoparticles in the apoferritin cavity by designing a slow chemical reaction system. Inorg Chem 44:6393–6400
24. Gálvez N, Sánchez P, Domínguez-Vera JM (2005) Preparation of Cu and CuFe prussian blue derivative nanoparticles using the apoferritin cavity as nanoreactor. Dalton Trans 2492–2494
25. Okuda M, Iwahori K, Yamashita I, Yoshimura H (2003) Fabrication of nickel and chromium nanoparticles using the protein cage of apoferritin. Biotech Bioeng 84:187–194
26. Chen G, Zhu X, Meng F, Yu Z, Li G (2008) Apoferritin as a bionanomaterial to facilitate the electron transfer reactivity of hemoglobin and the catalytic activity towards hydrogen peroxide. Bioelectrochemistry 72:77–80
27. Choi J-W, Kim YJ, Kim S-U, Min J, Oh B-K (2008) The fabrication of functional biosurface composed of iron storage protein, ferritin. Ultramicroscopy 108:1356–1359
28. Tsukamoto R, Iwahori K, Muraoka M, Yamashita I (2005) Synthesis of Co_3O_4 nanoparticles using the cage-shaped protein, apoferritin. Bull Chem Soc Jpn 78:2075–2081
29. Meldrum FC, Douglas T, Levi S, Arosio P, Mann S (1995) Reconstitution of manganese oxide cores in horse spleen and recombinant ferritins. J Inorg Biochem 58:59–68
30. Ueno T, Suzuki M, Goto T, Matsumoto T, Nagayama K, Watanabe Y (2004) Size-selective olefin hydrogenation by a Pd nanocluster provided in an apoferritin cage. Angew Chem Int Ed 43:2527–2530
31. Warne B, Kasyuich OI, Mayes EL, Wiggins JAL, Wong KKW (2000) Self assembled nanoparticle Co:Pt for data storage applications. IEEE Trans Magn 36:3009–3011
32. Wong KKW, Mann S (1996) Biomimetic synthesis of cadmium sulfide–ferritin nanocomposites. Adv Mater 8:928–932
33. Cherry RC, Bjornsen AJ, Zapien DC (1998) Direct electron transfer of ferritin adsorbed at tin-doped indium oxide electrodes. Langmuir 14:1971–1973
34. Pyon M-S, Cherry RJ, Bjornsen AJ, Zapien DC (1999) Uptake and release of iron by ferritin adsorbed at tin-doped indium oxide electrodes. Langmuir 15:7040–7046
35. Zapien DC, Johnson MA (2000) Direct electron transfer of ferritin adsorbed at bare gold electrodes. J Electroanal Chem 494:114–120
36. Shina KM, Leea JW, Wallace GG, Kima SJ (2008) Electrochemical properties of SWNT/ferritin composite for bioapplications. Sens Acuators B 133:393–397
37. Tominaga M, Ohira A, Yamaguchi Y, Kunitake M (2004) Electrochemical, AFM and QCM studies on ferritin immobilized onto a self-assembled monolayer-modified gold electrode. J Electroanal Chem 566:323–329
38. Kim J-W, Choi SH, Lillehei PT, Chu S-H, King GC, Watt GD (2007) Electrochemically controlled reconstitution of immobilized ferritins for bioelectronic applications. J Electroanal Chem 601:8–16
39. Won K, Park MJ, Yoon HH, Kim JH (2008) Immobilization of iron storage protein on a gold electrode based on self-assembled monolayers. Ultramicroscopy 108:1342–1347
40. Wu Y, Hu S (2004) Direct electron transfer of ferritin in dihexadecylphosphate on an Au film electrode and its catalytic oxidation toward ascorbic acid. Anal Chim Acta 527:37–43
41. Yoshizawa K, Iwahori K, Sugimoto K, Yamashita I (2006) Fabrication of gold nanoparticles using the protein cage of apo ferritin. Chem Lett 35:1192–1193
42. Allen M, Willits D, Young M, Douglas T (2003) Constrained synthesis of cobalt oxide nanomaterials in the 12-subunit protein cage from *Listeria innocua*. Inorg Chem 42:6300–6305
43. Douglas T, Stark VT (2000) Nanophase cobalt oxyhydroxide mineral synthesized within the protein cage of ferritin. Inorg Chem 39:1828–1830
44. Kim J-W, Choi SH, Lillehei PT, Chu S-H, King GC, Watt GW (2005) Cobal toxide hollow nanoparticles derived by bio-templating. Chem Commun 4101–4103
45. Stryer L (1965) The interaction of a naphthalene dye with apomyoglobin and apohemoglobin: a fluorescent probe of non-polar binding sites. J Mol Biol 13:482–495
46. Daniel E, Weber G (1966) Cooperative effects in binding by bovine serum albumin. I. The binding of 1-anilino-8-naphthalenesulfonate fluorimetric titrations. Biochemistry 5:1893–1900
47. Slavik J (1982) Anilinonaphthalene sulfonate as a probe of membrane composition and function. Biochim Biophys Acta 694:1–25
48. Kelly SM, Price NC (2000) The use of circular dichroism in the investigation of protein structure and function. Curr Prot Peptide Sci 1:349–384
49. Suna W, Wanga D, Li G, Zhai Z, Zhao R, Jiaoa K (2008) Direct electron transfer of hemoglobin in a CdS nanorods and nafion composite film on carbon ionic liquid electrode. Electrochim Acta 53:8217–8221
50. Han X, Cheng W, Zhang Z, Dong S, Wang E (2002) Direct electron transfer between hemoglobin and a glassy carbon electrode facilitated by lipid-protected gold nanoparticles. Biochim Biophys Acta 1556:273–277
51. Theil EC (1978) Ferritin: structure, gene regulation, and cellular function in animals, plants, and microorganisms. Annu Rev Biochem 56:289–315